

Symmetries and exponential error reduction in Yang-Mills theories on the lattice

Michele Della Morte and Leonardo Giusti

CERN, Physics Department, TH Division, CH-1211 Geneva 23, Switzerland

Abstract

The partition function of a quantum field theory with an exact symmetry can be decomposed into a sum of functional integrals each giving the contribution from states with definite symmetry properties. The composition rules of the corresponding transfer matrix elements can be exploited to devise a multi-level Monte Carlo integration scheme for computing correlation functions whose numerical cost, at a fixed precision and at asymptotically large times, increases power-like with the time extent of the lattice. As a result the numerical effort is exponentially reduced with respect to the standard Monte Carlo procedure. We test this strategy in the SU(3) Yang-Mills theory by evaluating the relative contribution to the partition function of the parity odd states.

1 Introduction

Dynamical properties of quantum field theories can be determined on the lattice by computing appropriate functional integrals via Monte Carlo simulations. For the most interesting theories this is, up to now, the only tool to carry out non-perturbative computations from first principles. The mass of the lightest asymptotic state with a given set of quantum numbers can, for instance, be extracted from the Euclidean time dependence of a suitable two-point correlation function. Its contribution can be disentangled from those of other states by inserting the source fields at large-enough time distances. The associated statistical error can be estimated from the spectral properties of the theory [1, 2]. Very often the latter grows exponentially with the time separation, and in practice it is not possible to find a window where statistical and systematic errors are both under control. This is a well known major limiting factor in many numerical computations such as, for example, the computation of the glueball masses in the Yang–Mills theory. A widely used strategy to mitigate this problem is to reduce the systematic error by constructing interpolating operators with a small overlap on the excited states [3, 4]. The lowest energy is then extracted at short time-distances by assuming a negligible contamination from excited states, sometimes also with the help of anisotropic lattices [5, 6]. This procedure is not entirely satisfactory from a conceptual and a practical point of view. The exponential problem remains unsolved, and the functional form of the sources are usually optimized so that the correlator shows a single exponential decay in the short time range allowed by the statistical noise. A solid evidence that a single state dominates the correlation function, i.e. a long exponential decay over many orders of magnitude, is thus missing.

In this paper we propose a computational strategy to solve the exponential problem. The latter arises in the standard procedure since for any given gauge configuration all asymptotic states of the theory are allowed to propagate in the time direction, regardless of the quantum numbers of the source fields. By using the transfer matrix formalism, we introduce projectors in the path integral which, configuration by configuration, permit the propagation in time of states with a given set of quantum numbers only. The composition properties of the projectors can then be exploited to implement a hierarchical multi-level integration procedure similar to those proposed in Refs. [7, 8] for the Polyakov loops. By iterating over several levels the numerical cost of computing the relevant observables grows, at asymptotically large times, with a power of the time extent of the lattice.

We test our strategy of a “symmetry constrained” Monte Carlo in the $SU(3)$ Yang–Mills theory by determining the relative contribution to the partition function of the parity-odd states on lattices with a spacing of roughly 0.17 fm, spatial volumes up to 2.5 fm^3 , and time extent up to 3.4 fm. The algorithm behaves as expected, and in particular the multi-level integration scheme achieves an exponential reduction of the numerical effort. In the specific numerical implementation adopted here the computation of the projectors is the most expensive part, and its cost scales roughly with the

square of the three-dimensional volume. The realistic lattices considered in this paper, however, were simulated with a modest computational effort.

The strategy proposed here is rather general and we expect it to be applicable to other symmetries and other field theories including those having fermions as fundamental degrees of freedom. It can, of course, be quite useful also for computing excited levels in other quantum mechanical systems. The basic ideas were indeed checked in a considerable simpler and solvable quantum system with a non-trivial parity symmetry, namely the one dimensional harmonic oscillator [9].

2 Preliminaries and basic notation

We set up the SU(3) Yang–Mills theory on a finite four-dimensional lattice of volume $V = T \times L^3$ with a spacing a and periodic boundary conditions¹. The gluons are discretized through the standard Wilson plaquette action

$$S[U] = \frac{\beta}{2} \sum_x \sum_{\mu, \nu} \left[1 - \frac{1}{3} \text{Re Tr} \left\{ U_{\mu\nu}(x) \right\} \right], \quad (2.1)$$

where the trace is over the color index, $\beta = 6/g_0^2$ with g_0 the bare coupling constant, and the plaquette is defined as a function of the gauge links $U_\mu(x)$ as

$$U_{\mu\nu}(x) = U_\mu(x) U_\nu(x + \hat{\mu}) U_\mu^\dagger(x + \hat{\nu}) U_\nu^\dagger(x), \quad (2.2)$$

with $\mu, \nu = 0, \dots, 3$, $\hat{\mu}$ is the unit vector along the direction μ and x is the space-time coordinate. The action is invariant under a gauge transformation

$$U_\mu(x) \longrightarrow U_\mu^\Omega(x) = \Omega(x) U_\mu(x) \Omega^\dagger(x + \hat{\mu}) \quad (2.3)$$

with $\Omega(x) \in \text{SU}(3)$. The path integral is defined as usual

$$Z = \int \mathcal{D}_4[U] e^{-S[U]}, \quad \mathcal{D}_4[U] = \prod_x \prod_{\mu=0}^3 \mathcal{D}U_\mu(x), \quad (2.4)$$

where $\mathcal{D}U$ is the invariant Haar measure on the SU(3) group, which throughout the paper will be always normalized such that $\int \mathcal{D}U = 1$. The average value of a generic operator \mathcal{O} can thus be written as

$$\langle \mathcal{O} \rangle = \frac{1}{Z} \int \mathcal{D}_4[U] e^{-S[U]} \mathcal{O}[U]. \quad (2.5)$$

¹Throughout the paper dimensionful quantities are always expressed in units of a .

2.1 Hilbert space

The Hilbert space of the theory is the space of all square-integrable complex-valued functions $\psi[V]$ of $V_k(\mathbf{x}) \in \text{SU}(3)$ with a scalar product defined as (\mathbf{x} is the three dimensional space-coordinate and $k = 1, 2, 3$)

$$\langle \phi | \psi \rangle = \int \mathbf{D}_3[V] \phi[V]^* \psi[V], \quad \mathbf{D}_3[V] = \prod_{\mathbf{x}} \prod_{k=1}^3 \mathcal{D}V_k(\mathbf{x}). \quad (2.6)$$

The ‘‘coordinate’’ basis is the set of vectors which diagonalize the field operator at all points \mathbf{x} , i.e.

$$\hat{V}_k(\mathbf{x})|V\rangle = V_k(\mathbf{x})|V\rangle, \quad (2.7)$$

and which are normalized such that

$$\langle V | \psi \rangle = \psi[V]. \quad (2.8)$$

From a quantum mechanical point of view, the field values $V_k(\mathbf{x})$ form the set of quantum numbers that label the vectors of the basis. In a gauge theory physical states are wave functions which satisfy

$$\psi[V^\Omega] = \psi[V] \quad (2.9)$$

for all gauge transformations Ω . A projector onto this subspace can be defined as

$$\langle V | \hat{P}_G | \psi \rangle = \int \mathbf{D}[\Omega] \psi[V^\Omega], \quad \mathbf{D}[\Omega] = \prod_{\mathbf{x}} \mathcal{D}\Omega(\mathbf{x}), \quad (2.10)$$

and it is straightforward to verify that $\hat{P}_G^2 = \hat{P}_G$.

2.2 Transfer matrix

The transfer matrix of a Yang-Mills theory discretized by the Wilson action has been constructed many years ago [10–13]. The subject is well known and it appears on text books, therefore we report only those formulæ which are relevant to the paper. The starting point is to rewrite the functional integral in Eq. (2.4) as

$$Z = \int \prod_{x_0=0}^{T-1} \mathbf{D}_3[V_{x_0}] \mathbb{T}[V_{x_0+1}, V_{x_0}] \quad (2.11)$$

where the transfer matrix elements are defined as

$$\mathbb{T}[V_{x_0+1}, V_{x_0}] = \int \mathbf{D}[\Omega] e^{-L[V_{x_0+1}, V_{x_0}, \Omega]}, \quad (2.12)$$

with

$$L[V_{x_0+1}, V_{x_0}] = K[V_{x_0+1}, V_{x_0}] + \frac{1}{2}W[V_{x_0+1}] + \frac{1}{2}W[V_{x_0}], \quad (2.13)$$

and Ω being identified with the link in the temporal direction. The kinetic and the potential contributions to the Lagrangian are given by

$$K[V_{x_0+1}, V_{x_0}] = \beta \sum_{\mathbf{x}, k} \left[1 - \frac{1}{3} \text{Re Tr} \left\{ V_k(x_0 + 1, \mathbf{x}) V_k^\dagger(x_0, \mathbf{x}) \right\} \right], \quad (2.14)$$

and

$$W[V_{x_0}] = \frac{\beta}{2} \sum_{\mathbf{x}} \sum_{k, l} \left[1 - \frac{1}{3} \text{Re Tr} \left\{ V_{kl}(x_0, \mathbf{x}) \right\} \right], \quad (2.15)$$

respectively, where V_{kl} is the plaquette defined in Eq. (2.2) computed with the links $V_k(\mathbf{x})$. The potential term is gauge-invariant, i.e. $W[V_{x_0}] = W[V_{x_0}^\Omega]$, while the dependence of the kinetic term on the gauge transformations Ω' at time $(x_0 + 1)$ and Ω at time x_0 is only via the product $\Omega^\dagger \Omega'$. Thanks to the invariance of the Haar measure under left and right multiplication, this implies that the transfer matrix is gauge-invariant

$$\mathbb{T}[V_{x_0+1}^{\Omega'}, V_{x_0}^\Omega] = \mathbb{T}[V_{x_0+1}, V_{x_0}], \quad (2.16)$$

and that

$$\mathbb{T}[V_{x_0+1}, V_{x_0}] = \int \mathbf{D}[\Omega'] \mathbf{D}[\Omega] e^{-L[V_{x_0+1}^{\Omega'}, V_{x_0}^\Omega]}. \quad (2.17)$$

The latter are thus matrix elements of a transfer operator $\hat{\mathbb{T}}$ between gauge invariant states

$$\mathbb{T}[V_{x_0+1}, V_{x_0}] = \langle V_{x_0+1} | \hat{\mathbb{P}}_G \hat{\mathbb{T}} \hat{\mathbb{P}}_G | V_{x_0} \rangle, \quad (2.18)$$

and the functional integral can then be written as

$$Z = \text{Tr} \left\{ \left[\hat{\mathbb{T}} \hat{\mathbb{P}}_G \right]^T \right\}, \quad (2.19)$$

where the trace is over all gauge invariant states. For a thick time-slice, i.e. the ensemble of points in the sub-lattice with time coordinates in a given interval $[x_0, y_0]$ and bounded by the equal-time hyper-planes at times x_0 and y_0 , the transfer matrix elements can be introduced by the formula

$$\mathbb{T}[V_{y_0}, V_{x_0}] = \int \prod_{w_0=x_0+1}^{y_0-1} \mathbf{D}_3[V_{w_0}] \prod_{z_0=x_0}^{y_0-1} \mathbb{T}[V_{z_0+1}, V_{z_0}]. \quad (2.20)$$

3 Decomposition of the functional integral

The invariance of the system under a global symmetry can be exploited to decompose the partition function into a sum of functional integrals each giving the contribution from states with definite symmetry properties. In the following we will focus on the invariance of the Yang–Mills theory under parity.

In the coordinate basis, the parity transformation on gauge invariant states can be defined as

$$\hat{\phi}|V\rangle = |V^\varphi\rangle, \quad |V\rangle = \hat{P}_G|V\rangle, \quad V_k^\varphi(\mathbf{x}) = V_k^\dagger(-\mathbf{x} - \hat{k}), \quad (3.1)$$

which implies that $\hat{\phi}^2 = \mathbb{1}$. The parity eigenstates can then be written as

$$|V, \pm\rangle = \frac{1}{\sqrt{2}} \left[|V\rangle \pm |V^\varphi\rangle \right], \quad \hat{\phi}|V, \pm\rangle = \pm|V, \pm\rangle. \quad (3.2)$$

and their transfer matrix elements are given by

$$\langle s', V_{x_0+1} | \hat{T} | V_{x_0}, s \rangle = 2\delta_{s's} \mathbf{T}^s[V_{x_0+1}, V_{x_0}], \quad (3.3)$$

$$\mathbf{T}^s[V_{x_0+1}, V_{x_0}] = \frac{1}{2} \left\{ \mathbf{T}[V_{x_0+1}, V_{x_0}] + s \mathbf{T}[V_{x_0+1}, V_{x_0}^\varphi] \right\}. \quad (3.4)$$

The invariance of the action yields

$$\mathbf{T}[V_{x_0+1}^\varphi, V_{x_0}^\varphi] = \mathbf{T}[V_{x_0+1}, V_{x_0}], \quad \mathbf{T}[V_{x_0+1}^\varphi, V_{x_0}] = \mathbf{T}[V_{x_0+1}, V_{x_0}^\varphi], \quad (3.5)$$

and therefore

$$\mathbf{T}^s[V_{x_0+1}, V_{x_0}^\varphi] = s \mathbf{T}^s[V_{x_0+1}, V_{x_0}]. \quad (3.6)$$

For a thick time-slice the matrix elements between parity states can be introduced by exploiting the composition rule

$$\mathbf{T}^s[V_{y_0}, V_{x_0}] = \left\{ \mathbf{T}^s[V_{y_0}, V_{z_0}] \mathbf{T}^s[V_{z_0}, V_{x_0}] \right\}, \quad (3.7)$$

where $x_0 < z_0 < y_0$ and in general

$$\left\{ \mathbf{T}^s[V_{y_0}, V_{z_0}] \mathbf{T}^{s'}[V_{z_0}, V_{x_0}] \right\} = \int \mathbf{D}_3[V_{z_0}] \mathbf{T}^s[V_{y_0}, V_{z_0}] \mathbf{T}^{s'}[V_{z_0}, V_{x_0}]. \quad (3.8)$$

It is easy to show that, in addition to relations analogous to those in Eqs. (3.4)–(3.6), the identities

$$\left\{ \mathbf{T}^s[V_{y_0}, V_{z_0}] \mathbf{T}^{-s}[V_{z_0}, V_{x_0}] \right\} = 0, \quad (3.9)$$

$$\left\{ \mathbf{T}^s[V_{y_0}, V_{z_0}] \mathbf{T}[V_{z_0}, V_{x_0}] \right\} = \mathbf{T}^s[V_{y_0}, V_{x_0}] \quad (3.10)$$

hold. In particular they imply that

$$\frac{\mathbf{T}^s[V_{y_0}, V_{x_0}]}{\mathbf{T}[V_{y_0}, V_{x_0}]} = \frac{1}{Z_{\text{sub}}} \int \mathbf{D}_4[U]_{\text{sub}} e^{-S[U]} \frac{\mathbf{T}^s[U_{y_0}, U_{y_0-1}]}{\mathbf{T}[U_{y_0}, U_{y_0-1}]}, \quad (3.11)$$

an useful expression for the practical implementation of the multi-level algorithm described in the following section. The subscript “sub” indicates that the integral is

performed over the dynamical field variables in the thick time-slice $[x_0, y_0]$ with the spatial components $U_k(x)$ of the boundary fields fixed to $V_k(x_0, \vec{x})$ and $V_k(y_0, \vec{x})$ respectively. Finally, by inserting Eq. (3.4) into Eq. (2.11) and repeatedly applying Eq. (3.9), it is possible to rewrite the path integral as a sum of functional integrals

$$Z = \sum_{s=\pm} Z^s, \quad Z^s = \int \prod_{x_0=0}^{T-1} \mathbf{D}_3[V_{x_0}] \mathbf{T}^s[V_{x_0+1}, V_{x_0}], \quad (3.12)$$

each giving the contribution from gauge-invariant parity-even and -odd states respectively

$$Z^+ = e^{-E_0 T} \left[1 + \sum_{n=1} w_n^+ e^{-E_n^+ T} \right], \quad Z^- = e^{-E_0 T} \sum_{m=1} w_m^- e^{-E_m^- T}. \quad (3.13)$$

In these expressions E_0 is the vacuum energy, E_n^+ and E_m^- are the energies (with respect to the vacuum one) of the parity even and odd eigenstates, and w_n^+ and w_m^- are the corresponding weights. The latter are integers and positive since for the Wilson action the transfer operator $\hat{\mathbf{T}}$ is self-adjoint and strictly positive [11].

It is interesting to notice that even though the transfer matrix formalism inspired the construction, the above considerations hold independently of the existence of a positive self-adjoint transfer operator. The insertion of $\mathbf{T}^s[V_{y_0}, V_{x_0}]$ in the path integral plays the rôle of a projector, as on each configuration it allows the propagation in the time direction of states with parity s only. Indeed the parity transformation of one of the boundary fields in $\mathbf{T}[V_{y_0}, V_{x_0}]$ flips the sign of all contributions that it receives from the parity-odd states while leaving invariant the rest. The very same applies to the path integral in Eq. (2.4) if the periodic boundary conditions are replaced by \wp -periodic boundary conditions, i.e. $V_T = V_0^\wp$. All contributions from the parity odd states are then multiplied by a minus sign. Similar considerations have already been exploited in different contexts, for instance in the study of the interface free energy of the three-dimensional Ising model [14].

4 Multi-level simulation algorithm

The composition rules in Eqs. (3.7)–(3.10) are at the basis of our strategy for computing Z^s/Z (as well as a generic correlation function) with a hierarchical multi-level integration procedure.

4.1 Projector computation

To determine the parity projector between two boundary fields of a thick time-slice, the basic building block to be computed is the ratio of transfer matrix elements

$$\mathbf{R}[V_{x_0+d}, V_{x_0}] = \frac{\mathbf{T}[V_{x_0+d}, V_{x_0}^\wp]}{\mathbf{T}[V_{x_0+d}, V_{x_0}]}. \quad (4.1)$$

The parity transformation in the numerator changes one of the boundary fields over the entire spatial volume of the corresponding time-slice, a global operation which could make the logarithm of this ratio proportional to the spatial volume, see for instance [14]. The transfer matrix formalism and the expected spectral properties of the Yang–Mills theory however suggest that, in a finite volume and for d large enough, only a few of the physical states give a sizeable contribution to this ratio, which is therefore expected to be of $O(1)$. These general properties can be studied analytically for the free lattice scalar theory, see for instance [15]. It goes without saying that the latter has a different spectrum from the Yang–Mills theory, and therefore can be used only as an example where our strategy can be studied analytically.

Even though the ratio R is expected to be of $O(1)$, the integrands in the numerator and in the denominator on the r.h.s of Eq. (4.1) are, in general, very different and the main contributions to their integrals come from different regions of the phase space. The most straightforward way for computing R is to define a set of n systems with partition functions $\mathcal{Z}_1 \dots \mathcal{Z}_n$ designed in such a way that the relevant phase spaces of successive integrals overlap and that $\mathcal{Z}_1 = \mathbb{T}[V_{x_0+d}, V_{x_0}^\varnothing]$ and $\mathcal{Z}_n = \mathbb{T}[V_{x_0+d}, V_{x_0}]$. The ratio R can then be calculated as

$$R = \frac{\mathcal{Z}_1}{\mathcal{Z}_2} \times \frac{\mathcal{Z}_2}{\mathcal{Z}_3} \times \dots \times \frac{\mathcal{Z}_{n-2}}{\mathcal{Z}_{n-1}} \times \frac{\mathcal{Z}_{n-1}}{\mathcal{Z}_n}, \quad (4.2)$$

with each ratio on the r.h.s. being computable in a single Monte Carlo simulation by averaging the proper reweighting factor. To implement this procedure we start by generalizing the definition of the transfer matrix element in Eq. (2.17) as

$$\bar{\mathbb{T}}[V_{x_0+1}, V_{x_0}, r] = \int \mathbf{D}[\Omega'] \mathbf{D}[\Omega] e^{-\bar{L}[V_{x_0+1}^{\Omega'}, V_{x_0}^{\Omega^\dagger}, r]}, \quad (4.3)$$

where $r \in [-1/2, 1/2]$ and

$$\begin{aligned} \bar{L}[V_{x_0+1}, V_{x_0}, r] &= \left(\frac{1}{2} + r\right) K[V_{x_0+1}, V_{x_0}] + \left(\frac{1}{2} - r\right) K[V_{x_0+1}^\varnothing, V_{x_0}] \\ &+ \frac{1}{2} W[V_{x_0+1}] + \frac{1}{2} W[V_{x_0}]. \end{aligned} \quad (4.4)$$

Analogously, Eq. (3.11) can be generalized as

$$\bar{\mathbb{T}}[V_{x_0+d}, V_{x_0}, r] = \int \prod_{w_0=x_0+1}^{x_0+d-1} \mathbf{D}_3[V_{w_0}] \left[\prod_{z_0=x_0}^{x_0+d-2} \mathbb{T}[V_{z_0+1}, V_{z_0}] \right] \bar{\mathbb{T}}[V_{x_0+d}, V_{x_0+d-1}, r] \quad (4.5)$$

and the ratio $R[V_{x_0+d}, V_{x_0}]$ can be written as

$$R[V_{x_0+d}, V_{x_0}] = \prod_{k=1}^{L^3} \bar{R}[V_{x_0+d}, V_{x_0}, -1/2 + (k-1/2)\varepsilon] \quad (4.6)$$

where

$$\overline{\mathbb{R}}[V_{x_0+d}, V_{x_0}, r] = \frac{\overline{\mathbb{T}}[V_{x_0+d}, V_{x_0}, r - \varepsilon/2]}{\overline{\mathbb{T}}[V_{x_0+d}, V_{x_0}, r + \varepsilon/2]} \quad (4.7)$$

and $\varepsilon = 1/L^3$. With this choice of ε the relevant phase spaces of two consecutive integrals overlap since the actions differ by a quantity of $O(1)$, while their fluctuations are of $O(\sqrt{V})$. To compute each ratio on the r.h.s. of Eq. (4.6) one starts by noticing that the group integrals on Ω' and Ω in Eq. (4.3) can be factorized by introducing on each point of the time-slice x_0 the usual temporal link $U_0(x_0, \vec{x}) = \Omega^\dagger(\vec{x})\Omega'(\vec{x})$ and a second temporal link $U_4(x_0, \vec{x}) = \Omega^\dagger(\vec{x})\Omega'(-\vec{x})$. The average of the reweighting factor is then computed with the three-level algorithm described in Appendix A. As other methods for computing ratios of partition functions which are present in the literature [16–18], the numerical cost scales roughly quadratically with the three-dimensional volume. Since the main goal of this paper is to present and test the validity of the strategy, we leave to future studies the development of a more refined and better scaling algorithm for the computation of the projector.

4.2 Hierarchical integration

Once the projectors have been computed, the ratio of partition functions Z^s/Z can be calculated by implementing the hierarchical two-level integration formula

$$\frac{Z^s}{Z} = \frac{1}{Z} \int \mathbb{D}_4[U] e^{-S[U]} \mathbb{P}_{m,d}^s[T, 0] \quad (4.8)$$

where $\mathbb{P}_{m,d}^s[y_0, x_0]$ is defined as

$$\mathbb{P}_{m,d}^s[y_0, x_0] = \prod_{i=0}^{m-1} \frac{\mathbb{T}^s[U_{x_0+(i+1)\cdot d}, U_{x_0+i\cdot d}]}{\mathbb{T}[U_{x_0+(i+1)\cdot d}, U_{x_0+i\cdot d}]} \quad (4.9)$$

with $m \geq 1$ and $y_0 = x_0 + m \cdot d$. The procedure can, of course, be generalized to a multi-level algorithm. For a three-level one, for instance, each ratio on the r.h.s of Eq. (4.9) can be computed by a two-level scheme. Thanks to the composition rules in Eqs. (3.7) and (3.9), the r.h.s. of Eq. (4.8) does not depend on m and d . When computed by a Monte Carlo procedure, however, its statistical error depends strongly on the specific form of $\mathbb{P}_{m,d}^s[y_0, x_0]$ chosen. The algorithm therefore requires an optimization which in general depends on the spectral properties of the theory. It is however important to stress that the multi-level hierarchical integration gives always the correct result independently on the details of its implementation. This can be shown by following the same steps in the Appendix A of Ref. [8]. There are two main differences: auxiliary link variables and their own actions need to be introduced for each value of r , and the computation of $\overline{\mathbb{R}}$ requires a thermalization procedure for each value of r . We do not expect the latter to be particularly problematic since, as mentioned earlier, expectation values for consecutive values of r refer to path integrals with the relevant phase spaces which overlap. The

ratios \overline{R} are computed by simulating systems corresponding to consecutive values of r one after the other, and by starting from the one used to extract the boundary fields ($r = 0.5$).

4.3 Exponential error reduction

The statistical variance of the estimate of a two-point correlation function $\langle O(x_0)O(0) \rangle$ of a parity-odd interpolating operator O , computed by the standard Monte Carlo procedure, is defined as

$$\sigma^2 = \langle O^2(x_0)O^2(0) \rangle - \langle O(x_0)O(0) \rangle^2 . \quad (4.10)$$

At asymptotically-large time separations the signal-to-noise ratio can be easily computed via the transfer matrix formalism which, for $0 \ll x_0 \ll T/2$, gives [1, 2]

$$\frac{\langle O(x_0)O(0) \rangle}{\sigma} = \frac{|\langle E_1^- | \hat{O} | 0 \rangle|^2}{|\langle 0 | \hat{O}^2 | 0 \rangle|} e^{-E_1^- x_0} + \dots \quad (4.11)$$

The exponential decrease of this ratio with the time distance can be traced back to the fact that for each gauge configuration the standard Monte Carlo allows for the propagation in time of all asymptotic states of the theory regardless of the quantum numbers of the source field O . Therefore each configuration gives a contribution to the signal which decreases exponentially in time, whereas it contributes $O(1)$ to the noise (variance) at any time distance. On the contrary, if in Eq. (4.8) d is chosen large enough for the single thick-slice ratio to be roughly dominated by the contribution of the lightest state, then each factor is of order $e^{-E_1^- d}$. For each configuration of the boundary fields, the magnitude of the product is proportional to $e^{-E_1^- T}$, and the statistical fluctuations are reduced to this level. To achieve an analogous exponential gain in the computation of the correlation functions, the projectors T^s have to be inserted in the proper way among the interpolating operators (see Ref. [9] for a more detailed discussion).

5 Numerical simulations

We have tested the hierarchical multi-level integration strategy described in the previous section for the SU(3) Yang–Mills theory by performing extensive numerical computations. We have simulated lattices with an inverse gauge coupling of $\beta = 6/g_0^2 = 5.7$ which corresponds to a value of the reference scale r_0 of about $2.93a$ [19, 20]. The number of lattice points in each spatial direction has been set to $L = 6, 8$ corresponding to a linear size of 1.0 and 1.4 fm respectively. For each spatial volume we have considered several time extents T , the full list is reported in Table 1 together with the number of configurations generated and the details of the multi-level simulation algorithm used for each run. The lattices have been chosen to test the strategy in a realistic situation with the computational resources at our disposal, i.e. a machine equivalent to approximately 6 dual processor quad-core PC nodes of the last generation running for a few months.

Lattice	L	T	N_{conf}	N_{lev}	d
A ₁	6	4	50	2	4
A ₂		5	50	2	5
A ₃		6	50	2	6
A ₄		8	175	2	4
A ₅		10	50	2	5
A ₆		12	90	2	6
A ₇		16	48	2	8
A ₈		20	48	3	{5,10}
B ₁	8	4	20	2	4
B ₂		5	25	2	5
B ₃		6	75	2	3
B ₄		8	48	2	4

Table 1: Simulation parameters: N_{conf} is the number of configurations of the uppermost level, N_{lev} is the number of levels and d is the thickness of the thick time-slice used for the various levels.

5.1 Algorithm implementation and tests

The basic Monte Carlo update of each link variable is a combination of heatbath and over-relaxation updates which implements the Cabibbo–Marinari scheme [21]. Depending on the value of the coupling constant associated to the link at a given stage of the simulation, the heatbath updates the SU(2) sub-matrices by the Metropolis, the Creutz [22] or the Fabricius–Haan [23, 24] algorithm. In the uppermost level the generation of the gauge field configurations consumes a negligible amount of computer time. At this level we perform many update cycles between subsequent configurations (typically 500 iterations of 1 heatbath and $L/2$ over-relaxation updates of all link variables) so that they can be assumed to be statistically independent. On each of these configurations we compute the “observables” $P_{m,d}^s[T, 0]$, with the most expensive part being the estimate of the thick-slice ratio $R[V_{x_0+d}, V_{x_0}]$ at the lowest algorithmic level. The latter is computed by using the three-level algorithm described in the previous section, with the parameter values tuned sequentially level by level so to minimize the actual CPU cost for the required statistical precision. In all runs this has been set to be at most 30% of the expected absolute value of the deviation of R from 1, the latter being determined by some preliminary exploratory tests. As mentioned in section 4.2, the algorithm requires a thermalization step for each value of r which has been fixed, after several exploratory runs, to 500 sweeps of the full sub-lattice.

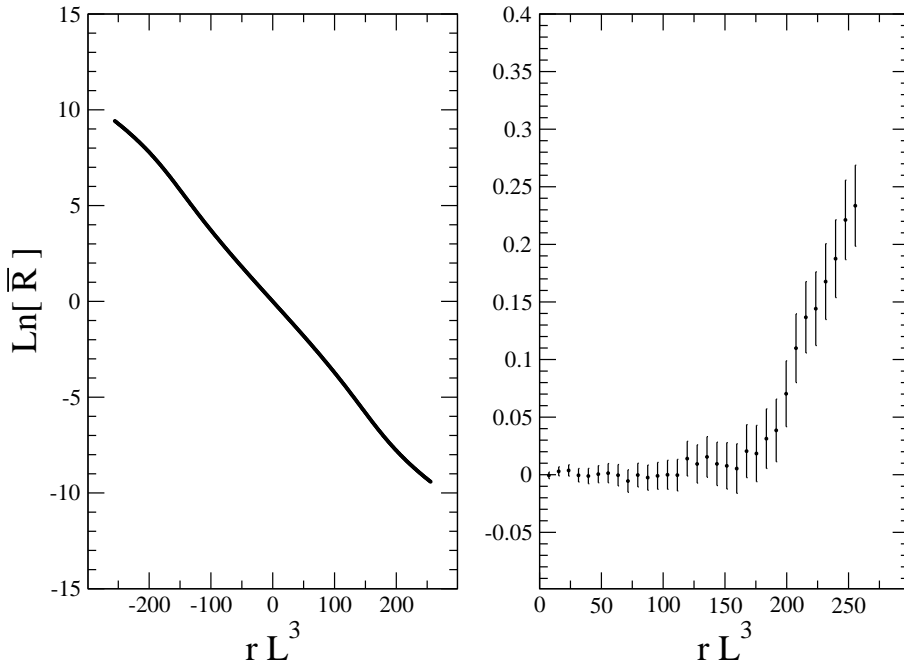


Figure 1: Left: the natural logarithm of $\overline{\mathbb{R}}[V_{x_0+d}, V_{x_0}, r]$ is shown as a function of r (statistical errors are smaller than symbols) for a typical configuration of the run B_3 . Right: the sum of the points in the interval $[-r, r]$ is plotted as a function of r (one each eighth point for visual convenience).

Apart from many consistency checks of the programs, we have verified several non-trivial properties of the basic ratios in Eqs. (4.1) and (4.7). We have monitored the deviation from the equality

$$\overline{\mathbb{R}}[V_{x_0+d}, V_{x_0}^\varphi, r] = \overline{\mathbb{R}}[V_{x_0+d}, V_{x_0}, -r]^{-1} \quad (5.1)$$

for several boundary configurations and all values of r , and it turns out to be compatible with being a Gaussian statistical fluctuation. For the runs with $d = T$ we have verified that, on each configuration and within the statistical error, the ratio $\mathbb{T}^-[V_T, V_0]/\mathbb{T}[V_T, V_0]$ is always positive as predicted by the transfer matrix representation. For $d = T/2$ the two thick-slice ratios in Eq. (4.8) have to be equal. We have monitored the difference in a significant sample of our configurations, and it turns out to be compatible with a Gaussian statistical fluctuation as well.

The natural logarithm of $\overline{\mathbb{R}}[V_{x_0+d}, V_{x_0}, r]$ is shown as a function of r in the left panel of Fig. 1 for a typical configuration of the run B_3 . As expected, its value is of $O(1)$ for each value of r . Its almost perfect asymmetry under $r \rightarrow -r$, however, makes the sum of all the L^3 points a quantity of $O(1)$. This impressive cancellation, which is at work for $T > 3$ on both volumes, can be better appreciated in the right panel of

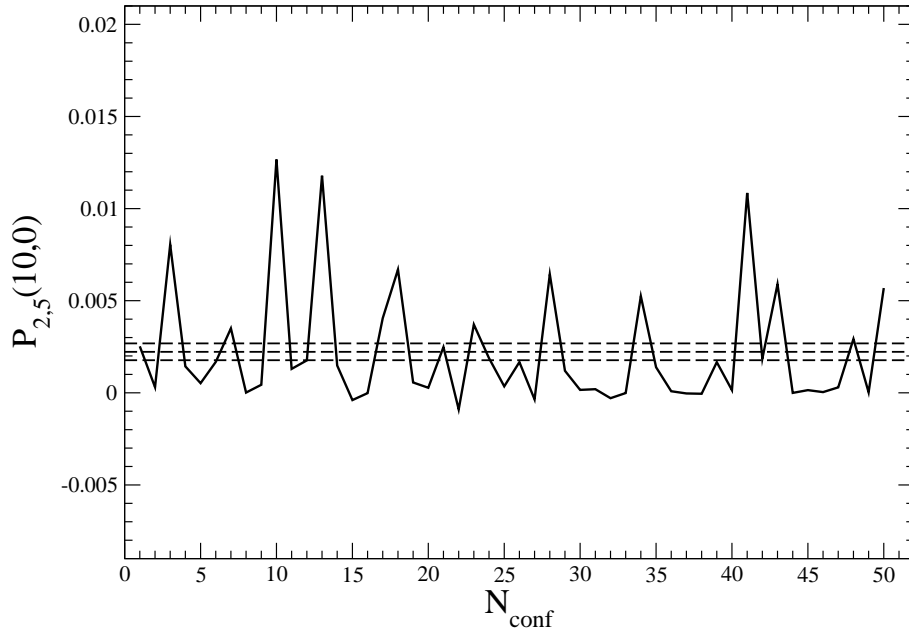


Figure 2: Monte Carlo history of the quantity $P_{2,5}^-[10,0]$ for the run A_5 . The central dashed line corresponds to the average value, while the other two delimit the one standard deviation region.

the same Figure, where the sum of the function in the interval $[-r, r]$ is plotted for a subset of values of r . It is the deviation from the exact asymmetry which flips in sign under a parity transformation of one of the boundary fields, and forms the signal we are interested in. A similar behaviour is observed for all other configurations and runs.

The Monte Carlo history of $P_{2,T/2}^-[T,0]$ is shown in Figure 2 for the lattice A_5 . Also for all other runs we have observed reasonable Monte Carlo histories, and therefore we have computed Z^s/Z and its statistical error in the standard way. The run A_4 however is much noisier than the others, with rather large fluctuations due to a few configurations. This could be related to the fact that $d = 4$ is not yet large enough, and sizeable contaminations from the heavier states amplify the statistical fluctuations. To check our statistical errors, we have also carried out a more refined analysis following Ref. [25]. No autocorrelations among configurations have been observed, and the errors are fully compatible with those of the standard analysis.

Before describing the main numerical results of the paper we mention that, for the runs where $m = 2$ is available, we have computed the quantity on the r.h.s of Eq. (3.9). As expected, it turns out to be always compatible with zero.

Lattice	$\frac{Z_{1,T}^+}{Z}$	$\frac{Z_{1,T}^-}{Z}$	$\frac{Z_{1,T/2}^+}{Z}$	$\frac{Z_{2,T/2}^+}{Z}$	$\frac{Z_{1,T/2}^-}{Z}$	$\frac{Z_{2,T/2}^-}{Z}$	M^-
A ₁	0.591(8)	0.409(8)	-	-	-	-	0.223(5)
A ₂	0.823(13)	0.177(13)	-	-	-	-	0.346(14)
A ₃	0.931(7)	0.069(7)	-	-	-	-	0.446(17)
A ₄	-	-	0.995(9)	1.004(20)	0.005(9)	$1.47(28) \cdot 10^{-2}$	0.528(24)
A ₅	-	-	1.003(7)	1.009(14)	-0.003(7)	$2.2(5) \cdot 10^{-3}$	0.611(20)
A ₆	-	-	0.998(3)	0.996(5)	0.002(3)	$6.6(17) \cdot 10^{-4}$	0.610(21)
A ₇	-	-	1.0006(9)	1.0012(17)	-0.0006(9)	$2.8(8) \cdot 10^{-5}$	0.655(18)
A ₈	-	-	0.9988(20)	0.998(4)	0.00024(20)	$1.5(5) \cdot 10^{-6}$	0.670(15)
B ₁	0.574(8)	0.426(8)	-	-	-	-	0.213(5)
B ₂	0.939(6)	0.061(6)	-	-	-	-	0.558(21)
B ₃	-	-	0.979(15)	0.97(3)	0.021(15)	$1.65(26) \cdot 10^{-2}$	0.685(27)
B ₄	-	-	0.997(5)	0.995(11)	0.003(5)	$1.37(26) \cdot 10^{-3}$	0.824(24)

Table 2: Numerical results for various primary observables and for M^- (see text).

5.2 Simulation results

The ratios Z^s/Z have been computed for all values of m available in each run by using Eq. (4.8). The results are collected in Table 2, where they are identified by the obvious notation $Z_{m,d}^s/Z$.

On each lattice the different determinations of $Z_{m,d}^s/Z$ are in good agreement, and the sum $(Z^+/Z + Z^-/Z)$ is always consistent with 1. For Z^-/Z a clear statistical signal is obtained for $m = 2$ only, and the larger error at $m = 1$ indicates that the exponential reduction of the noise is working as expected. To better appreciate the efficiency of the method, it is useful to define the quantity

$$M^- = -\frac{1}{T} \text{Ln} \left[\frac{Z^-}{Z} \right] \quad (5.2)$$

whose values are reported in Table 2. With the exception of the lattice A₄, it is clear that $O(50)$ measurements are enough to obtain a precision on M^- of the order of 5% on both spatial volumes. Sticking to the A lattices, the comparison of the relative errors on M^- at $T = 5, 6, 10, 12$ and at $T = 20$ indicates that the multi-level integration indeed achieves an exponential reduction of the noise. The most precise determination of Z^-/Z at each value of T is plotted in Fig. 3. Its value decreases by more than five orders of magnitude over the time range spanned. The symmetry constrained Monte Carlo clearly allows to follow the exponential decay over many orders of magnitude, a fact which represents one of the main results of the paper.

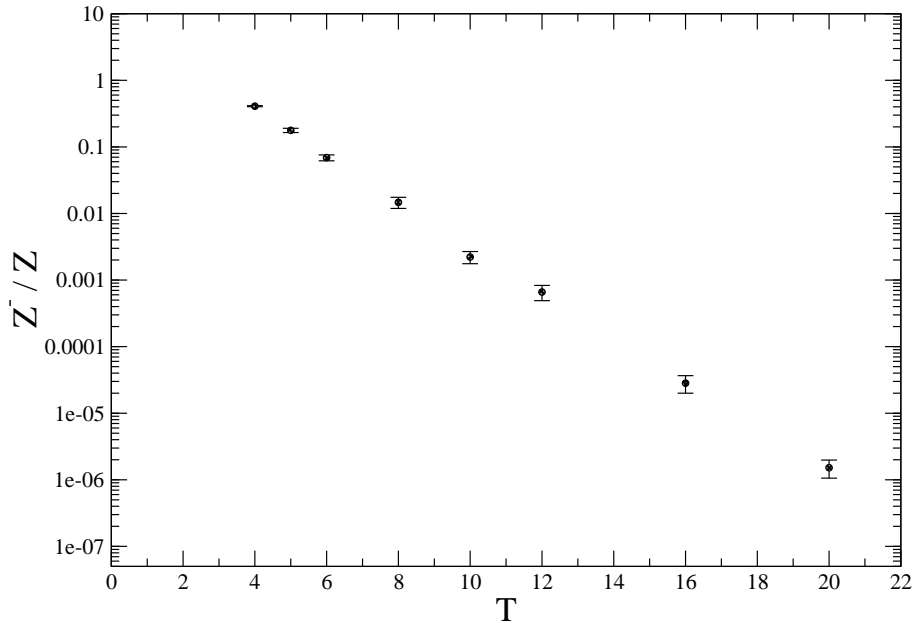


Figure 3: The quantity Z^-/Z as a function of T .

The data in Table 2 confirm the expectation that at these volumes the ratio Z^-/Z suffers from large finite-size effects. If we enforce the theoretical prejudice that a single state with multiplicity 1 dominates Z^-/Z for large T , then M^- can be interpreted as an effective parity-odd glueball mass, which should approach its asymptotic value from below. Indeed this is verified at both values of L , as shown in Fig. 4 for the A lattices.

6 Conclusions

The exponential growth of the statistical error with the time separation of the sources is the main limiting factor for computing many correlators on the lattice by a standard Monte Carlo procedure. The integration scheme proposed here solves this problem by exploiting the symmetry properties of the underlying quantum theory, and it leads to an exponential reduction of the statistical error. In particular the cost of computing the energy of the lowest state in a given symmetry sector grows linearly with the time extent of the lattice.

In extensive simulations of the SU(3) Yang–Mills theory, we have observed a definite exponential reduction of the statistical error in the computation of the relative contribution of the parity-odd states to the partition function. The simulations needed at larger volumes and finer lattice spacings to provide a theoretically solid evidence for the presence of a glueball state, and to precisely determine its mass are now feasible with the present generation of computers.

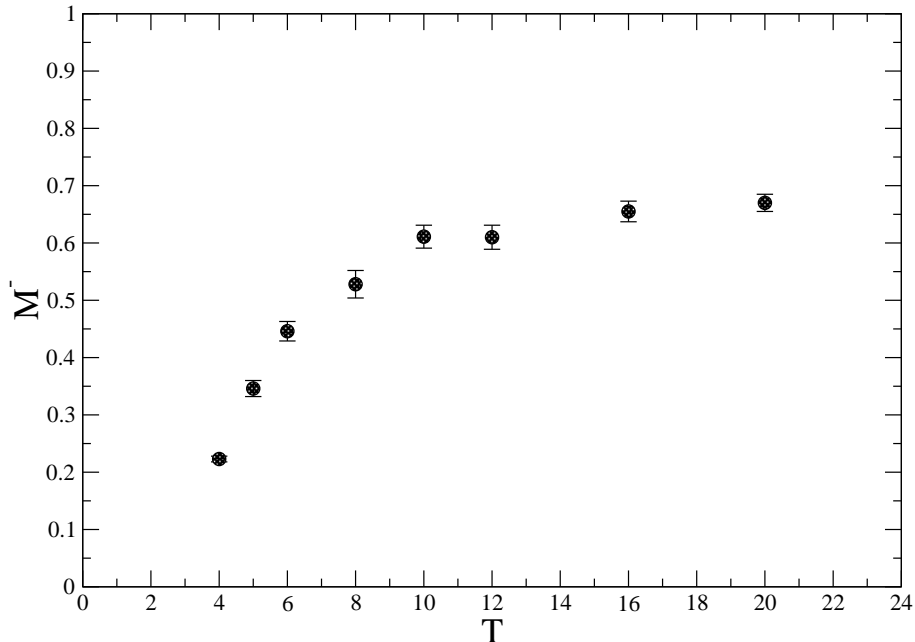


Figure 4: The effective mass M^- as a function of T .

Since the strategy is rather general, we expect it to be applicable to other symmetries and other field theories including those with fermions as fundamental degrees of freedom. In QCD, for instance, the very same problem occurs already in the computation of rather simple quantities such as the energy of the vector meson resonance, and it becomes even more severe for the η' and baryon masses. The approach presented here offers a new perspective for tackling these problems on the lattice.

The integration scheme described is yet another example of how the properties of the underlying quantum system, namely the parity symmetry, can be exploited to design more efficient exact numerical algorithms for the computation of the dynamical properties of the theory.

Acknowledgments

We thank Martin Lüscher for many illuminating discussions, for a careful reading of the first version of the manuscript, and for the constant encouragement throughout the last year. Our simulations were performed on PC clusters at the University of Bern, at CILEA, and at the University of Rome “La Sapienza”. We thankfully acknowledge the

computer resources and technical support provided by all these institutions and their technical staff.

A Numerical computation of $\bar{\mathbf{R}}$

In this Appendix we describe how the ratio $\bar{\mathbf{R}}[V_{x_0+d}, V_{x_0}, r]$, defined in Eq. (4.7), has been computed by a three-level algorithm. The partition function $\bar{\mathbf{T}}[V_{x_0+d}, V_{x_0}, r]$ is rewritten as

$$\bar{\mathbf{T}}[V_{x_0+d}, V_{x_0}, r] = \int \mathbf{D}_4[U]_{\text{sub}} \mathbf{D}[U_4] e^{-\bar{\mathbf{S}}[U, r]}, \quad (\text{A.1})$$

where a second temporal link $U_4(y_0, \vec{y})$ has been added to the standard degrees of freedom at each point of the time-slice $y_0 = (x_0 + d - 1)$. The subscript ‘‘sub’’ indicates the integration over the standard active-link variables of the thick time-slice $[x_0, x_0 + d]$ with the spatial components $U_k(x)$ of the boundary fields fixed to $V_k(x_0, \vec{x})$ and $V_k(x_0 + d, \vec{x})$ respectively. The modified action $\bar{\mathbf{S}}[U, r]$ reads

$$\bar{\mathbf{S}}[U, r] = S[U] + \frac{\beta}{6} (1 - 2r) \sum_{\vec{y}, k} \text{Re Tr} \left\{ U_{0k}(y_0, \vec{y}) - U_{4k}(y_0, \vec{y}) \right\}, \quad (\text{A.2})$$

where $U_{0k}(y)$ is defined in Eq. (2.2) and

$$U_{4k}(y) = U_4(y_0, \vec{y}) U_k^\dagger(y_0 + 1, -\vec{y} - \vec{k}) U_4^\dagger(y_0, \vec{y} + \hat{k}) U_k^\dagger(y_0, \vec{y}). \quad (\text{A.3})$$

If one defines the ‘‘reweighting’’ observable as

$$O[U, r + \varepsilon/2] = e^{\bar{\mathbf{S}}[U, r + \varepsilon/2] - \bar{\mathbf{S}}[U, r - \varepsilon/2]}, \quad (\text{A.4})$$

then the ratio $\bar{\mathbf{R}}[V_{x_0+d}, V_{x_0}, r]$ can be computed as its expectation value on the ensemble of gauge configurations generated with the action $\bar{\mathbf{S}}[U, r + \varepsilon/2]$. In practice the average value of the observable O is estimated by implementing the following three-level algorithm:

1. Generate a thermalized configuration with the action $\bar{\mathbf{S}}[U, r + \varepsilon/2]$ by spanning the sub-lattice with several sweeps of the update algorithm (see section 5.1);
2. Compute an estimate of $\langle O \rangle$ by averaging over n_0 (level 0) configurations² generated by keeping fixed all link variables with the exception of the links U_0 and U_4 on the time-slice y_0 ;
3. Repeat step 2 over n_1 (level 1) configurations generated by keeping fixed all links of the sub-system with the exception of those on the time-slice y_0 , and average over the results obtained;

²Notice that when spatial links are kept fixed, the set of U_0 and U_4 factorize and are generated independently.

4. Repeat step 3 over n_2 (level 2) configurations generated by updating all links of the sub-lattice with the action $\overline{S}[U, r + \varepsilon/2]$, and average over the results obtained.

At each level the numbers n_0 , n_1 and n_2 of configurations generated are chosen to minimize the numerical cost required to reach the desired statistical precision. Their values depend on d and r . In the simulations that we have carried out they range in the intervals $n_0 = 12 - 50$, $n_1 = 50 - 120$ and $n_2 = 50 - 300$.

References

- [1] G. Parisi, Phys. Rept. 103 (1984) 203.
- [2] G.P. Lepage, TASI 89 Summer School, Boulder, CO, Jun 4-30, 1989.
- [3] M. Albanese et al., Phys. Lett. B192 (1987) 163.
- [4] M. Teper, Phys. Lett. B183 (1987) 345.
- [5] C.J. Morningstar and M.J. Peardon, Phys. Rev. D56 (1997) 4043, hep-lat/9704011.
- [6] C.J. Morningstar and M.J. Peardon, Phys. Rev. D60 (1999) 034509, hep-lat/9901004.
- [7] G. Parisi, R. Petronzio and F. Rapuano, Phys. Lett. B128 (1983) 418.
- [8] M. Lüscher and P. Weisz, JHEP 09 (2001) 010, hep-lat/0108014.
- [9] M. Della Morte and L. Giusti, CERN-PH-TH-2007-196.
- [10] K.G. Wilson, in "New developments in quantum field theory and statistical mechanics", Cargèse 1976, Eds. M. Lévy and P. Mitter, Plenum (NY 1977).
- [11] M. Lüscher, Commun. Math. Phys. 54 (1977) 283.
- [12] M. Creutz, Phys. Rev. D15 (1977) 1128.
- [13] K. Osterwalder and E. Seiler, Ann. Phys. 110 (1978) 440.
- [14] M. Caselle, M. Hasenbusch and M. Panero, JHEP 09 (2007) 117, 0707.0055.
- [15] H.J. Rothe, World Sci. Lect. Notes Phys. 59 (1997) 1.
- [16] A.M. Ferrenberg and R.H. Swendsen, Phys. Rev. Lett. 63 (1989) 1195.
- [17] C. Hoelbling, C. Rebbi and V.A. Rubakov, Phys. Rev. D63 (2001) 034506, hep-lat/0003010.
- [18] P. de Forcrand, M. D'Elia and M. Pepe, Phys. Rev. Lett. 86 (2001) 1438, hep-lat/0007034.

- [19] ALPHA Coll., M. Guagnelli, R. Sommer and H. Wittig, Nucl. Phys. B535 (1998) 389, hep-lat/9806005.
- [20] S. Necco and R. Sommer, Nucl. Phys. B622 (2002) 328, hep-lat/0108008.
- [21] N. Cabibbo and E. Marinari, Phys. Lett. B119 (1982) 387.
- [22] M. Creutz, Phys. Rev. D21 (1980) 2308.
- [23] K. Fabricius and O. Haan, Phys. Lett. B143 (1984) 459.
- [24] A.D. Kennedy and B.J. Pendleton, Phys. Lett. B156 (1985) 393.
- [25] ALPHA, U. Wolff, Comput. Phys. Commun. 156 (2004) 143, hep-lat/0306017.